

Quantum mechanical description of excitation energy distribution of the reaction residue in nucleon-induced inclusive one-nucleon knockout reactions

Kazuyuki Ogata^{1,*}

¹Research Center for Nuclear Physics (RCNP), Osaka University, Ibaraki 567-0047, Japan

(Dated: September 21, 2018)

Background: Understanding of inclusive one-nucleon knockout reactions for long-lived fission fragments (LLFPs) is crucial for nuclear transmutation studies. However, the particle and heavy ion transport code system (PHITS) severely overshoots the inclusive one-nucleon knockout cross sections σ_{-1N} .

Purpose: Development of a reaction model for describing the inclusive one-nucleon knockout processes is necessary. A key is specification of the position and the momentum of a nucleon inside a nucleus to be struck by the incident nucleon.

Methods: The semiclassical distorted wave model incorporating the Wigner transform of the one-body nuclear density matrix is applied to the calculation of excitation energy distributions of reaction residues. Decay of a residue is described by introducing a threshold parameter for the minimum excitation energy of it.

Results: With reasonable values of the parameter, the measured σ_{-1N} for several LLFPs are reproduced by the proposed reaction model. The incident energy dependence of σ_{-1N} is found to be governed by that of the nucleon-nucleon cross sections at energies higher than about 75 MeV. At low energies, the nuclear absorption and the Coulomb penetrability also become important. The energy dependence of neutron-induced σ_{-1N} is predicted and found to be quite different from that of proton induced one.

Conclusions: The proposed reaction model is shown to be promising in discussing the energy dependence of nucleon-induced inclusive one-nucleon knockout processes. The energy dependence of the measured σ_{-1p} for ¹⁰⁷Pd above 100 MeV is, however, not explained by the present calculation.

I. INTRODUCTION

Reduction of high-level radioactive wastes produced in nuclear power plants is one of the most crucial issues in modern society. As a possible solution, so far a great effort has been devoted to realize the nuclear transmutation technology [1]. Very recently, nuclear spallation cross sections for some long-lived fission products (LLFPs), which are very important reaction data for nuclear transmutation, have been measured for the first time at the RIKEN RI Beam Factory (RIBF) [2–4]. However, it is very difficult to measure the cross section data for all LLFPs at various incident energies. We therefore need a reliable model that can describe the existing data and has a predictive power. The particle and heavy ion transport code system (PHITS) [5] is one of the most promising candidates for “a standard model” to evaluate not only cross sections for specific reaction processes but also the amount of reaction products of a macroscopic system. In fact, PHITS has successfully been applied to facility design, medical physics, radiation production, and geoscience.

It was found that in general PHITS reproduces well the spallation cross sections taken at RIBF with hydrogen and deuterium targets. However, for processes in which only one nucleon is removed, PHITS tends to significantly overshoot the cross sections in many cases. It was discussed in Ref. [6] that overshooting of one-nucleon knockout cross sections by the Liège intranuclear cascade (INCL) model [7, 8], which is incorporated in PHITS, comes from the nucleon momentum distribution inside a nucleus adopted by the model. In the INCL model a nucleon in the nuclear surface must have higher

momentum, being in direct contradiction to the picture of the local Fermi-gas model. As a result, after a nucleon-nucleon collision that knocks out one nucleon, the excitation energy of the reaction residue has to be too low to allow further particle emission. The one-nucleon knockout cross sections evaluated with the INCL model are thus significantly larger than the experimental data. Very recently, a similar overshooting was reported [9] for the spallation cross sections of p -¹³⁶Xe at 200 MeV/nucleon taken at GSI. In Ref. [6] a phenomenological prescription to ease the restriction on nucleon momentum distributions in the nuclear surface was proposed, which improved the agreement between the result of the INCL model and experimental data. Thus, the nucleon momentum distribution inside a nucleus is found to be a key for evaluating one-nucleon knockout cross sections.

In this paper I propose a quantum-mechanical reaction model for describing one-nucleon knockout processes, with incorporating the Wigner transform (WT) of the one-body density matrix (OBDM) as a distribution of positions and momenta of a nucleon inside a nucleus. The reaction model is based on the semiclassical distorted wave (SCDW) model [10–16] developed for describing inclusive (p, p') and (p, n) processes to the continuum. Although the SCDW model can include up to three-step processes in terms of the nucleon-nucleon collision, in this paper I take into account only a one-step process. This limitation will not significantly affect the discussion on one-nucleon knockout processes, because these occur only when a reaction residue has excitation energy in a narrow window that allows a reaction system to emit just one nucleon. Multistep direct processes hardly satisfy the condition required, at least for kinematics with which a meaningfully large cross section is obtained.

It should be noted that the reaction model proposed in this study is different from a usual distorted wave impulse ap-

*kazuyuki@rcnp.osaka-u.ac.jp

proximation (DWIA) [17–19]. The DWIA assumes a single-particle (s.p.) wave function for the struck nucleon, and evaluates a triple-differential cross section, momentum distribution of the residual nucleus, or an integrated cross section, for a nucleon knockout process. These observables are multiplied by the so-called spectroscopic factor S_{sp} for the s.p. state of interest and compared with data; in some cases through comparison with data S_{sp} is determined. This model is expected to work when the experiment is designed to observe a s.p. state (or some specific s.p. states) of a nucleus. In such measurement, usually the residual nucleus B is in the ground state or low-lying bound excited states. On the other hand, in the spallation process what is probed is no longer pure s.p. states, that is, inclusive measurement of s.p. structures. In other words, reaction processes in which B is in continuum states play a crucial role. As described below, inclusion of the WT of the OBDM as in Ref. [14] allows one to describe the nuclear many-body system in a suitable manner to calculate continuous excitation energy distribution of the reaction residue.

This paper is organized as follows. In Sec. II I introduce a reaction model for describing inclusive one-nucleon knockout processes. In Sec. III A numerical inputs are given and in Sec. III B I discuss the excitation energy distribution of reaction residues. The energy dependence of proton-induced one-nucleon knockout cross sections are shown in Sec. III C and those for neutron-induced reactions are discussed in Sec. III D. Finally, a summary is given in Sec. IV.

II. FORMALISM

In what follows, unless otherwise denoted, formulation is done in the center-of-mass (c.m.) frame. For simplicity I adopt nonrelativistic kinematics; in the actual numerical calculation a relativistic correction on the kinematics is included. I consider nucleon (N) induced inclusive processes, ($N, N'x$), where x represents that all the final states except for the outgoing nucleon are not specified. I assume the projectile nucleon is the same as the ejectile. This particle is called a leading particle (LP).

In the semiclassical distorted wave (SCDW) model incorporating the WT of the OBDM, the double differential cross section (DDX) for ($N, N'x$), with the outgoing energy E_f and the solid angle Ω_f specified, is given by [14]

$$\begin{aligned} \frac{d^2\sigma}{dE_f d\Omega_f} &= C \int d\mathbf{R} d\mathbf{k}_\beta d\mathbf{k}_\alpha \delta(\mathbf{K}_f + \mathbf{k}_\beta - \mathbf{K}_i - \mathbf{k}_\alpha) \\ &\times \left| \chi_{f, \mathbf{K}_f}^{(-)}(\mathbf{R}) \right|^2 \left[2 - f_h^{(\beta)}(\mathbf{k}_\beta, \mathbf{R}) \right] \\ &\times \left| \tilde{t}(\boldsymbol{\kappa}', \boldsymbol{\kappa}) \right|^2 f_h^{(\alpha)}(\mathbf{k}_\alpha, \mathbf{R}) \left| \chi_{i, \mathbf{K}_i}^{(+)}(\mathbf{R}) \right|^2 \\ &\times \delta(E_f + \varepsilon_\beta - E_i - \varepsilon_\alpha), \end{aligned} \quad (1)$$

where

$$C = \frac{\mu_f \mu_i}{(2\pi\hbar^2)^2} \frac{K_f}{K_i} \frac{1}{(2\pi)^3} \frac{1}{2} \quad (2)$$

is the kinematical factor; μ_c ($c = i$ or f) is the reduced mass in the initial (i) or final (f) channel and K_c is the asymptotic momentum of the LP in channel c . The distorted wave of the LP in the entrance (exit) channel, which is solved under an outgoing (incoming) boundary condition, is denoted by $\chi_{i, \mathbf{K}_i}^{(+)}$ ($\chi_{f, \mathbf{K}_f}^{(-)}$). \mathbf{k}_α and \mathbf{k}_β are what one may interpret as the momenta of the nucleon N_t inside the target nucleus A (the target nucleon) before and after the collision, respectively, with the LP.

\tilde{t} represents the matrix element of a nucleon-nucleon effective interaction calculated with the relative momentum $\boldsymbol{\kappa}$ ($\boldsymbol{\kappa}'$) of the colliding two nucleons in the initial (final) state; \tilde{t} is related to the nucleon-nucleon cross section ($d\sigma/d\Omega$) $_{NN_t}$ as

$$\left| \tilde{t}(\boldsymbol{\kappa}', \boldsymbol{\kappa}) \right|^2 = \frac{(2\pi\hbar^2)^2}{\mu_{NN_t}^2} \left(\frac{d\sigma}{d\Omega} \right)_{NN_t}, \quad (3)$$

where μ_{NN_t} is the reduced mass of the two nucleons.

The initial and final states of the nucleus are denoted by α and β , respectively, and these labels are understood to specify also whether the target nucleon is proton or neutron. $f_h^{(\gamma)}$ ($\gamma = \alpha$ or β) is the WT of the OBDM for hole states:

$$f_h^{(\gamma)}(\mathbf{k}_\gamma, \mathbf{R}) \equiv \sum_{nlj} \frac{2j+1}{2l+1} F_{nlj} f_{nlj}(\mathbf{k}_\gamma, \mathbf{R}) \quad (4)$$

with

$$\begin{aligned} f_{nlj}(\mathbf{k}_\gamma, \mathbf{R}) &\equiv \int d\mathbf{u} e^{-i\mathbf{k}_\gamma \cdot \mathbf{u}} \sum_m \varphi_{nlmj}^*(\mathbf{R} - \mathbf{u}/2) \\ &\times \varphi_{nlmj}(\mathbf{R} + \mathbf{u}/2). \end{aligned} \quad (5)$$

Here, φ_{nlmj} is the spatial part of a single-particle (s.p.) wave function specified by the principal quantum number n , the orbital angular momentum l , its third component m , and the total angular momentum j . The summation in Eq. (4) is taken over all the occupied states of the target nucleon. We adopt the filling approximation for an open orbit; F_{nlj} is the ratio of the number of nucleons in the orbit to $2j+1$. It is known that WT satisfies the following sum rule

$$f_h^{(\gamma)}(\mathbf{k}_\gamma, \mathbf{R}) + f_p^{(\gamma)}(\mathbf{k}_\gamma, \mathbf{R}) = 2, \quad (6)$$

where $f_p^{(\gamma)}$ is the WT for particle states. This sum rule has been used in deriving Eq. (1) and $2 - f_h^{(\beta)}$ appears accordingly. For more details, readers are referred to Ref. [14].

It should be noted that in Eq. (1) I have made a further approximation to the original SCDW model, that is, use of the asymptotic momentum \mathbf{K}_c instead of its local momentum in describing the kinematics of the LP inside A. The local momentum for the LP [10] is one of the most essential ingredients of the SCDW model, which allows the LP to reach a classically-inaccessible region and collide with a target nucleon there. Consequently, DDXs at very forward and backward angles change significantly as well as those with large energy transfer. However, in these regions the DDX is much smaller than its maximum value. A cross section integrated

over E_f and Ω_f , which we are interested in as discussed below, is hardly affected by the inclusion of the local momentum of the LP.

A noteworthy feature of the SCDW model is that the DDX is given as an incoherent sum over the coordinate \mathbf{R} , that is, the localization of the nucleon-nucleon collision inside A. This allows one to define *the collision point* of reaction processes, which gives in part a theoretical foundation to classical and quantum-mechanical simulations, such as the INC model [6–8, 20], quantum molecular dynamics (QMD) [21], and the time-dependent version of antisymmetrized molecular dynamics (AMD) [22], applied to nuclear reaction studies. With the smoothness approximation to the WT, which was justified in Ref. [14], the s.p. energy ε_γ is evaluated by

$$\varepsilon_\gamma = \frac{\hbar^2}{2m_{N_t}} k_\gamma^2 + U_{N_t}(R), \quad (7)$$

where m_{N_t} is the mass of the target nucleon and U_{N_t} is the s.p. potential; for proton U_{N_t} includes the Coulomb interaction. We then define the following quadruple ‘‘cross section’’

$$\begin{aligned} \frac{d^4\sigma}{dE_f d\Omega_f dk_\alpha dR} &= C \frac{k_\alpha m_{N_t}}{\hbar^2 q} \int d\phi_\alpha \int R^2 d\Omega_R \left| \chi_{f, \mathbf{K}_f}^{(-)}(\mathbf{R}) \right|^2 \\ &\times \left[2 - f_h^{(\beta)}(\mathbf{k}_\beta, \mathbf{R}) \right] \left| \tilde{t}(\boldsymbol{\kappa}', \boldsymbol{\kappa}) \right|^2 \\ &\times f_h^{(\alpha)}(\mathbf{k}_\alpha, \mathbf{R}) \left| \chi_{i, \mathbf{K}_i}^{(+)}(\mathbf{R}) \right|^2, \quad (8) \end{aligned}$$

where q is the magnitude of the momentum transfer $\mathbf{q} = \mathbf{K}_i - \mathbf{K}_f$, Ω_R is the solid angle of \mathbf{R} , and ϕ_α is the azimuthal angle of \mathbf{k}_α with respect to \mathbf{q} . Through Eq. (7), ε_α is determined by R and k_α . Thus one may construct

$$\begin{aligned} \frac{d^2\sigma}{dE_f d\varepsilon_\alpha} &\equiv f_{\text{id}} \int d\Omega_f dk_\alpha dR \frac{d^4\sigma}{dE_f d\Omega_f dk_\alpha dR} \\ &\times \delta \left(\frac{\hbar^2}{2m_{N_t}} k_\gamma^2 + U_{N_t}(R) - \varepsilon_\alpha \right) \\ &= \frac{d^2\sigma}{d\omega d\varepsilon_\alpha}, \quad (9) \end{aligned}$$

where ω is the energy transfer defined by

$$\omega = E_i - E_f = \varepsilon_\beta - \varepsilon_\alpha. \quad (10)$$

In Eq. (9) f_{id} is a normalization factor for nucleon-nucleon cross sections; it is 1/2 (unity) when the LP is identical to (different from) the target nucleon,

Here I consider two possibilities for the residual nucleus, which is called the pre-fragment (PF) in PHITS, to be followed by particle decay. One is the nucleus A – N_t referred to as B, and the other is A. The first case is realized when i) ε_β is larger than the barrier height $\varepsilon_{\text{br}N_t}$ for the struck nucleon and ii) the intrinsic energy of B

$$\varepsilon_{\text{ex}}^{\text{B}} \equiv -S_{N_t}^{\text{A}} - \varepsilon_\alpha, \quad (11)$$

where $S_{N_t}^{\text{A}}$ is the nucleon separation energy of A, is larger than a threshold energy ε_{0N_t} . $\varepsilon_{\text{br}N_t}$ is taken to be the maximum value of U_{N_t} ; for neutron $\varepsilon_{\text{br}N_t} = 0$. Since $\varepsilon_{\text{ex}}^{\text{B}}$ can be

interpreted as excitation energy of B, ideally it should be positive and ε_{0N_t} is set to 0. However, in this study I use ε_{0N_t} as an adjustable parameter to reproduce one-nucleon knockout cross sections measured at some specific energies. Necessity of introducing ε_{0N_t} will be due to lack of understanding of nuclear structure wave functions and also to inadequacy of the interpretation of \mathbf{k}_γ as a momentum of the target nucleon, that is, Eq. (7).

Once B is adopted as the PF, its excitation energy distribution is obtained by

$$\frac{d\sigma^{(\text{PF:B})}}{d\varepsilon_{\text{ex}}^{\text{B}}} = \int d\omega d\varepsilon_\alpha \frac{d^2\sigma^{(\text{PF:B})}}{d\omega d\varepsilon_\alpha} \delta(-S_{N_t}^{\text{A}} - \varepsilon_\alpha - \varepsilon_{\text{ex}}^{\text{B}}), \quad (12)$$

where

$$\frac{d^2\sigma^{(\text{PF:B})}}{d\omega d\varepsilon_\alpha} \equiv \frac{d^2\sigma}{d\omega d\varepsilon_\alpha} \Theta(\varepsilon_\beta - \varepsilon_{\text{br}N_t}) \Theta(\varepsilon_{\text{ex}}^{\text{B}} - \varepsilon_{0N_t}) \quad (13)$$

with Θ being the Heaviside function. Unless the conditions i) and ii) are both satisfied, the nucleus A is chosen as the PF, and its excitation energy distribution is given following the definition of ω by

$$\frac{d\sigma^{(\text{PF:A})}}{d\varepsilon_{\text{ex}}^{\text{A}}} = \int d\varepsilon_\alpha \frac{d^2\sigma^{(\text{PF:A})}}{d\omega d\varepsilon_\alpha} \quad (14)$$

with

$$\begin{aligned} \frac{d^2\sigma^{(\text{PF:A})}}{d\omega d\varepsilon_\alpha} &\equiv \frac{d^2\sigma}{d\omega d\varepsilon_\alpha} \\ &\times \left[1 - \Theta(\varepsilon_\beta - \varepsilon_{\text{br}N_t}) \Theta(\varepsilon_{\text{ex}}^{\text{B}} - \varepsilon_{0N_t}) \right]. \quad (15) \end{aligned}$$

Rigorously speaking, the decaying property of the PF should be described by a statistical model. For example, one can export $d\sigma^{(\text{PF:C})}/d\varepsilon_{\text{ex}}^{\text{C}}$ (C is A or B) to the code system CCONe [23] and obtain one-nucleon knockout cross sections σ_{-1N} . Instead of this, I just employ a threshold rule to calculate σ_{-1N} in the following manner. When the PF is B, I calculate

$$\sigma_{-1N_t}^{(\text{PF:B})} \equiv \int_{\varepsilon_{0N_t}}^{S_{\text{min}}^{\text{B}}} d\varepsilon_{\text{ex}}^{\text{B}} \frac{d\sigma^{(\text{PF:B})}}{d\varepsilon_{\text{ex}}^{\text{B}}} \quad (16)$$

with

$$S_{\text{min}}^{\text{B}} \equiv \min(S_n^{\text{B}}, S_p^{\text{B}}). \quad (17)$$

The upper limit $S_{\text{min}}^{\text{B}}$ of the integration is set so as not to occur further particle decay. On the other hand, when the PF is A,

$$\bar{\sigma}_{-1N_t}^{(\text{PF:A})} \equiv \int_{S_{N_t}^{\text{A}}}^{S_{N_t}^{\text{A}} + S_{\text{min}}^{\text{B}}} d\varepsilon_{\text{ex}}^{\text{A}} \frac{d\sigma^{(\text{PF:A})}}{d\varepsilon_{\text{ex}}^{\text{A}}} \quad (18)$$

is evaluated. Then for proton I estimate a Coulomb penetration probability $P_{\text{A}}^{\text{Coul}}$ with the WKB approximation, with averaging out its energy dependence between 0 and $S_{\text{min}}^{\text{B}}$ for the

proton energy. The contributions of the events in which the PF is A to the one-nucleon knockout cross sections read

$$\sigma_{-1p}^{(\text{PF:A})} = \frac{P_A^{\text{Coul}}}{1 + P_A^{\text{Coul}}} \bar{\sigma}_{-1p}^{(\text{PF:A})}, \quad (19)$$

$$\sigma_{-1n}^{(\text{PF:A})} = \bar{\sigma}_{-1n}^{(\text{PF:A})} + \frac{1}{1 + P_A^{\text{Coul}}} \bar{\sigma}_{-1p}^{(\text{PF:A})}. \quad (20)$$

σ_{-1N} ($N = p$ or n) is given by

$$\sigma_{-1N} = \sigma_{-1N}^{(\text{PF:A})} + \sigma_{-1N}^{(\text{PF:B})}. \quad (21)$$

III. RESULTS AND DISCUSSION

A. Numerical inputs

I employ the Dirac phenomenology [24] to calculate the optical potentials for the LP; the so-called EDAD1 parameter set is used. The s.p. wave functions for the nucleon inside A is calculated with the Woods-Saxon potential by Bohr and Mottelson [25]. The nonlocal correction proposed by Perey and Buck [26] is included on both the distorted waves of the LP and the s.p. wave functions of the target nucleon. The range of nonlocality is taken to be 0.85 fm.

Although it is not explicitly shown in the formulae in Sec. II, an R -dependent nucleon effective mass $m_{N_t}^*$, its so-called k -mass component, is adopted in the numerical calculation as in Ref. [16]. The geometry of the difference between $m_{N_t}^*$ and the bare mass m_{N_t} is assumed to be the same as that of the Bohr-Mottelson potential. The ratio $m_{N_t}^*/m_{N_t}$ at the center of the nucleus is taken to be 0.7 (0.8) for proton (neutron), referring Mahaux and Sartor [27].

As for \tilde{t} , I adopt the t -matrix interactions of Franey and Love [28], with the so-called final-energy prescription in making an on-shell approximation. \tilde{t} is, as defined, evaluated in the nucleon-nucleon c.m. frame, and multiplied by the Møller factor to be transformed to the nucleon-nucleus c.m. frame. The neutron-neutron cross section is assumed to be the same as the proton-proton one.

B. Excitation energy distribution

In Fig. 1(a) I show by the solid line $d\sigma^{(\text{PF:}^{92}\text{Zr})}/d\varepsilon_{\text{ex}}^{92}\text{Zr}$ for $^{93}\text{Zr}(p, p'x)$ at 100 MeV/nucleon, without considering the condition on $\varepsilon_{\text{ex}}^{92}\text{Zr}$. In other words, the result corresponds to the limit of $\varepsilon_{0n} \rightarrow -\infty$. This limit is always taken when I show excitation energy distributions below. The contributions from $R = 2-4$, 4-6, and 6-8 fm are shown by the dashed, dotted, and dash-dotted lines, respectively. In Fig. 1(b) the momentum distribution \mathfrak{N}_n , which can be obtained by integrating the WT over \mathbf{R} , of neutron in A is shown by the solid line. I use the normalization

$$\int dk_\alpha \mathfrak{N}_n(k_\alpha) = \mathcal{N}_A, \quad (22)$$

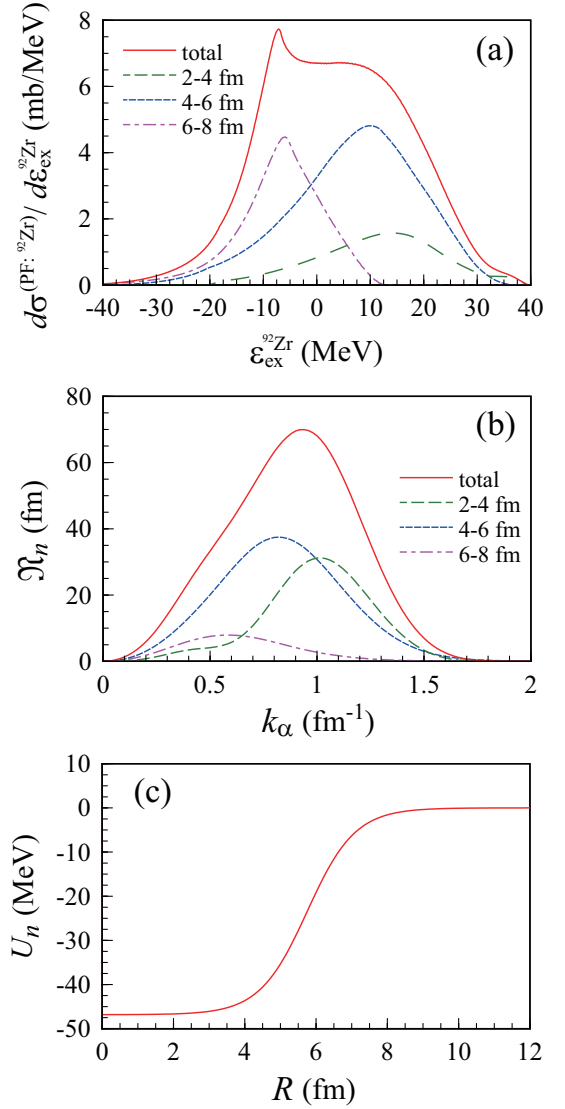


FIG. 1: (Color online) (a) Excitation energy distribution of ^{92}Zr after $^{93}\text{Zr}(p, p'x)$ at 100 MeV (solid line). The dashed, dotted, and dash-dotted lines show the contributions from the $R = 2-4$, 4-6, and 6-8 fm regions, respectively. (b) Neutron momentum distribution in ^{93}Zr (solid line); the meaning of the other three lines is the same as in (a). (c) Neutron single-particle potential.

where \mathcal{N}_A is the neutron number of A; $\mathcal{N}_A = 53$ in this case. The other three lines in Fig. 1(b) represent the contributions from the three regions of R . The correspondence between the lines and the R regions is the same as in Fig. 1(a). The neutron s.p. potential U_n is plotted in Fig. 1(c).

The dashed line in Fig. 1(b) has a peak at $k_\alpha \sim 1.0 \text{ fm}^{-1}$, whereas the dotted and dash-dotted ones at about 0.8 and 0.6 fm^{-1} , respectively. This is consistent with the picture of the local Fermi-gas model, that is, the upper limit of the nucleon momentum is restricted by the local density in which the nucleon exits. It should be noted that in the INCL model [7, 8] the nucleon momentum distribution in a nucleus is assumed

to be almost opposite to the results in Fig. 1(b); in the nuclear surface a nucleon has to have high momenta. A modification on this assumption was proposed in Ref. [6], which allows the nucleon to have a lower momentum. This is more consistent with the result obtained with the WT of the OBDM. However, there remains a somewhat large difference between the momentum distributions in Ref. [6] and Fig. 1(b).

Neutron at smaller R thus has larger kinetic energies. On the other hand, U_n becomes deeper as R decreases as shown in Fig. 1(c). For $R = 2-4$, the kinetic energy at the peak of \mathfrak{N}_n is about 25 MeV, whereas $U_n \sim -47$ MeV; note that $m_{N_t}^*/m_{N_t} \sim 0.8$ in this region. Consequently, through Eq. (11) with $S_n^{93\text{Zr}} = -8.28$ MeV, $d\sigma^{(\text{PF};92\text{Zr})}/d\varepsilon_{\text{ex}}^{92\text{Zr}}$ has a peak at around 14 MeV. If we go larger R , both the kinetic energy and the depth of U_n becomes smaller. Because the R -dependence of the latter is stronger, at large R , ε_α can be positive and even exceed $S_n^{93\text{Zr}}$. As a result, $d\sigma^{(\text{PF};92\text{Zr})}/d\varepsilon_{\text{ex}}^{92\text{Zr}}$ has a peak at negative $\varepsilon_{\text{ex}}^{92\text{Zr}}$, as shown by the dash-dotted line in Fig. 1(a). Furthermore, even though the dashed and dotted lines in Fig. 1(a) have a peak at positive $\varepsilon_{\text{ex}}^{92\text{Zr}}$, they are broad enough to have non-negligible cross sections for negative $\varepsilon_{\text{ex}}^{92\text{Zr}}$.

In Fig. 2 I show the results for the case in which a target nucleon is proton, in the same way as in Fig. 1. The proton momentum distribution \mathfrak{N}_p is similar to \mathfrak{N}_n in Fig. 1(b); the difference in the magnitude reflects that between the proton and neutron numbers of ^{93}Zr . The excitation energy distribution $d\sigma^{(\text{PF};92\text{Y})}/d\varepsilon_{\text{ex}}^{92\text{Y}}$ in Fig. 2(a) is found to be slightly shifted to lower energies, compared with $d\sigma^{(\text{PF};92\text{Zr})}/d\varepsilon_{\text{ex}}^{92\text{Zr}}$ in Fig. 1(a). This is mainly due to the Coulomb interaction in U_p that increases ε_α . One finds the absolute value of $d\sigma^{(\text{PF};92\text{Y})}/d\varepsilon_{\text{ex}}^{92\text{Y}}$ is somewhat smaller than that of $d\sigma^{(\text{PF};92\text{Zr})}/d\varepsilon_{\text{ex}}^{92\text{Zr}}$. This comes from not only the difference between the proton and neutron numbers of ^{93}Zr but also that between the proton-proton and proton-neutron total cross sections.

Interpretation of $d\sigma^{(\text{PF};\text{B})}/d\varepsilon_{\text{ex}}^{\text{B}}$, where B is ^{92}Zr or ^{92}Y , for negative excitation energies is not so trivial. In this study, as mentioned in Sec. II, I introduce ε_{0N_t} as a lower limit of the integration, above which $d\sigma^{(\text{PF};\text{B})}/d\varepsilon_{\text{ex}}^{\text{B}}$ contribute to $\sigma_{-1N_t}^{(\text{PF};\text{B})}$. I show in Table I ε_{0n} and ε_{0p} determined so as to reproduce the experimental values of $\sigma_{-1n}^{(\text{PF};\text{B})}$ and $\sigma_{-1p}^{(\text{PF};\text{B})}$. It should be noted that $\sigma_{-1p}^{(\text{PF};\text{B})}$ is governed by ε_{0p} , whereas $\sigma_{-1n}^{(\text{PF};\text{B})}$ is by not only ε_{0n} but also ε_{0p} through the neutron emission from A after a pp collision. In some cases ε_{0N_t} is found to be positive. This also will indicate inadequacy of understanding of the properties of nuclear many-body systems in the continuum. Nevertheless, ε_{0N_t} is found to lie in a reasonable range, except ε_{0p} for $^{107}\text{Pd}(p, p'x)$ at 196 MeV.

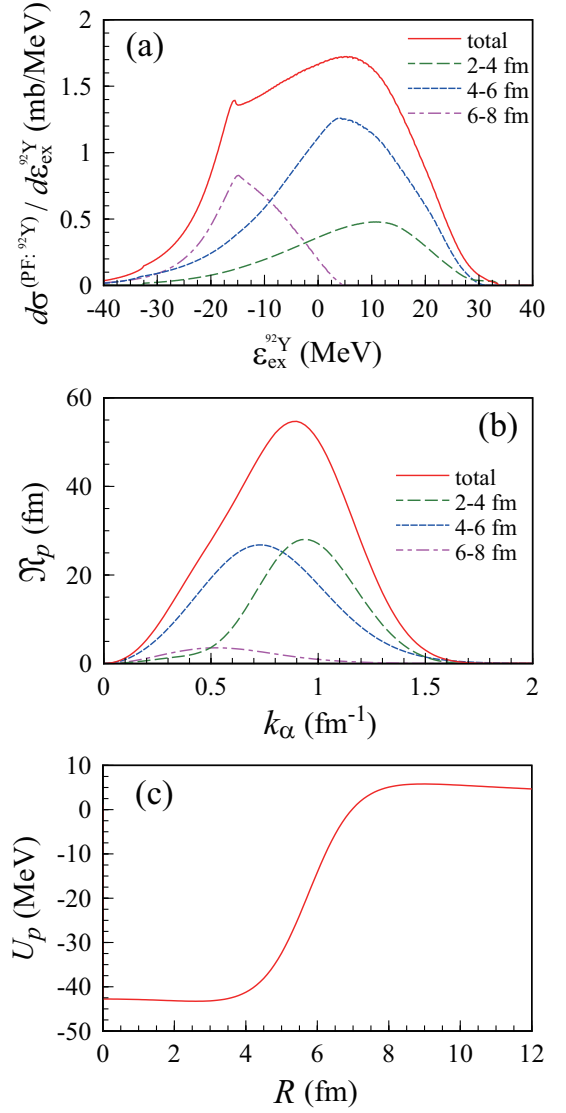


FIG. 2: (Color online) Same as in Fig. 1 but for ^{92}Y and for proton in ^{93}Zr .

C. Energy dependence of proton-induced one-nucleon knockout cross sections

I show in Fig. 3 the dependence of (a) σ_{-1n} and (b) σ_{-1p} on the incident energy E_{in} for $^{93}\text{Zr}(p, p'x)$. The circles are the experimental data [4] and the triangles are calculated results. The dots represent the contributions of $\sigma_{-1N}^{(\text{PF};93\text{Zr})}$ corresponding to the mean values of σ_{-1N} . I put a width of ε_{0p} and ε_{0n} corresponding to the uncertainties of the experimental data, and thereby estimate theoretical uncertainties. For visibility in the plot I slightly shift the energy of the results at 100 MeV; a similar shift is done also in the following when needed. One sees from Fig. 3 that for $E_{\text{in}} \geq 75$ MeV σ_{-1n} and σ_{-1p} decrease gradually as E_{in} increases, whereas they drop rather steeply at lower incident energy.

This energy dependence can qualitatively be understood

TABLE I: Threshold parameters ε_{0n} and ε_{0p} in unit of MeV. The experimental data for one-nucleon knockout cross sections used in the parameter fitting are taken from the references shown in the table.

	ε_{0n}	ε_{0p}	reference
$^{90}\text{Sr}@185\text{MeV}$	$-6.8^{+1.3}_{-1.2}$	$-3.2^{+1.6}_{-1.8}$	[2]
$^{93}\text{Zr}@100\text{MeV}$	$-3.0^{+0.9}_{-0.9}$	$3.3^{+1.3}_{-1.3}$	[4]
$^{107}\text{Pd}@196\text{MeV}$	$-9.2^{+1.2}_{-1.4}$	$-10.9^{+1.2}_{-1.2}$	[3]
$^{107}\text{Pd}@118\text{MeV}$	$-8.8^{+0.6}_{-0.6}$	$-2.6^{+1.2}_{-1.7}$	[3]
$^{137}\text{Cs}@185\text{MeV}$	$-5.7^{+1.4}_{-1.5}$	$5.1^{+2.2}_{-1.5}$	[2]

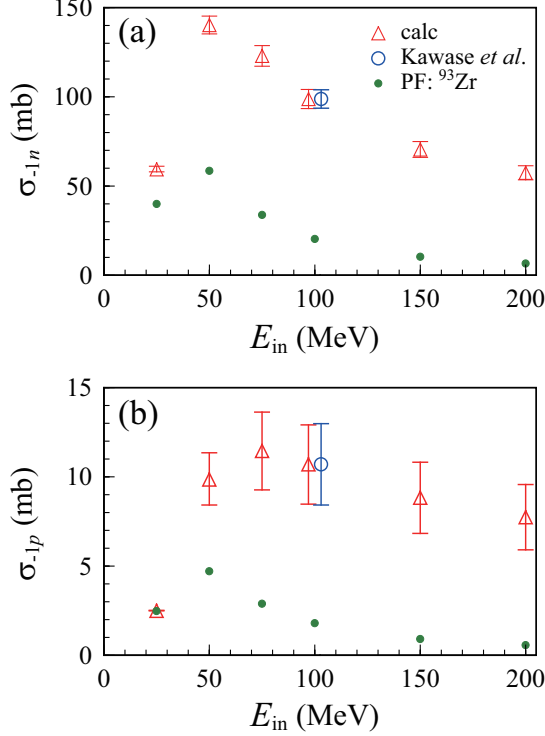


FIG. 3: (Color online) One-neutron (σ_{-1n}) and one-proton (σ_{-1p}) inclusive knockout cross sections (triangles) for $^{93}\text{Zr}(p, p'x)$, as a function of the incident energy E_{in} . The dots represent the contributions of the process in which the pre-fragment (PF) is ^{93}Zr . The experimental data (circles) are taken from Ref. [4].

as follows. Let us describe the proton-induced one-nucleon knockout process for a nucleus A with a $p + B + N_t$ three-body model. We first make the adiabatic approximation to the $B + N_t$ motion. Then we assume that the elastic breakup process, in which B is in the ground state after breakup, can be neglected. In this case, as one sees from Eqs. (17) and (18) of Ref. [29],

$$\sigma_{-1N_t} \approx \sigma_R(A) - \sigma_R(B), \quad (23)$$

where $\sigma_R(C)$ is the proton total reaction cross section for the nucleus C. Thus, the energy dependence of σ_{-1N_t} is essentially determined by that for the $p-N_t$ cross section σ_{pN_t} . At

low energies, as $\sigma_R(C)$ does, σ_{-1N_t} drops steeply because of the Coulomb barrier. For the description of the behavior at low energies, however, one needs a more quantitative analysis.

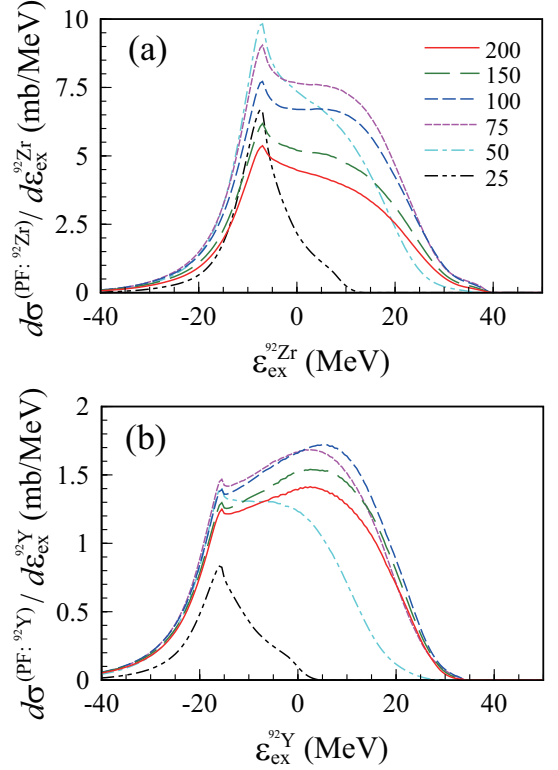


FIG. 4: (Color online) (a) Excitation energy distribution of ^{92}Zr after $^{93}\text{Zr}(p, p'x)$ at 100 MeV. The solid, long-dashed, dashed, dotted, dash-dotted, and dash-dot-dotted lines correspond to $E_{in} = 200, 150, 100, 75, 50,$ and 25 MeV, respectively. (b) Same as (a) but for ^{92}Y .

Figure 4 shows (a) $d\sigma^{(\text{PF: } ^{92}\text{Zr})}/d\varepsilon_{ex}^{92}\text{Zr}$ and (b) $d\sigma^{(\text{PF: } ^{92}\text{Y})}/d\varepsilon_{ex}^{92}\text{Y}$. In each panel, the solid, long-dashed, dashed, dotted, dash-dotted, and dash-dot-dotted lines represent the results at $E_{in} = 200, 150, 75, 50,$ and 25 MeV, respectively. For $E_{in} \gtrsim 75$ MeV, the shape of the distributions does not change significantly, whereas the absolute values monotonically decrease. The derivative for the decrease with respect to E_{in} in panel (a) is somewhat larger than that in panel (b). This is consistent with the energy dependence of σ_{pp} and σ_{pn} in the energy region.

Below 75 MeV, the distributions in the positive excitation energy region decrease rather steeply. At such low energies the energy transfer is not large enough to knockout a deeply bound nucleon that has small values of ε_{α} . This restriction is more significant for proton because of the Coulomb barrier. The E_{in} dependence of the absolute values around the peaks are determined by that of σ_{pN_t} and of the absorption due to the imaginary part of the optical potential for proton. As a result of the competition between these, for ^{92}Zr (^{92}Y) the peak height decreases E_{in} lower than 50 MeV (75 MeV). It should be noted, however, that to understand the energy dependence

of σ_{-1N} at low energies, the contributions of $\sigma_{-1N}^{(\text{PF}; ^{92}\text{Zr})}$ also must be taken into consideration.

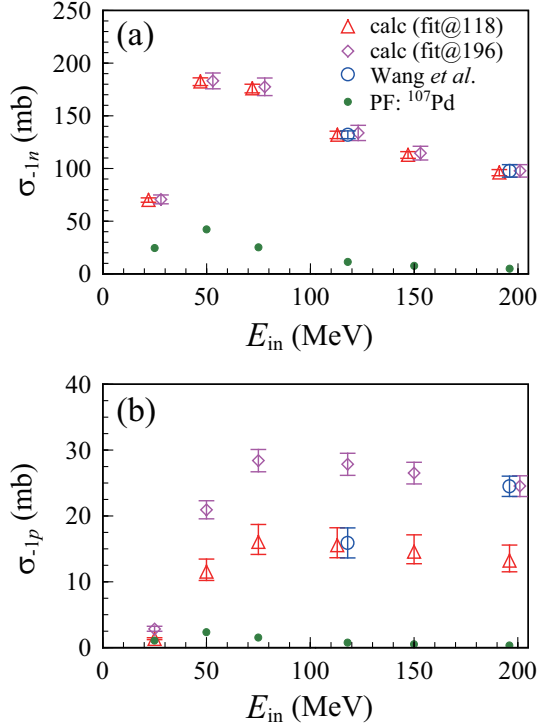


FIG. 5: (Color online) Same as Fig. 3 but for $^{107}\text{Pd}(p, p'x)$. The triangles (diamonds) represent the results calculated with ε_{0n} and ε_{0p} determined so as to reproduce the data at 118 MeV (196 MeV). The experimental data are taken from Ref. [3].

In Fig. 5 I show the E_{in} dependence of (a) σ_{-1n} and (b) σ_{-1p} for $^{107}\text{Pd}(p, p'x)$. The circles show the experimental data taken from Ref. [3]. The triangles (diamonds) represent the calculated results with the threshold parameters (ε_{0n} , ε_{0p}) determined so as to reproduce the experimental values at 118 MeV (196 MeV). Features of the results are the same as in Fig. 3. An important remark on this system is that for σ_{-1n} the two sets of theoretical results with different choices of (ε_{0n} , ε_{0p}) agree well with each other. This indicates that the E_{in} dependence of σ_{-1n} is well described by the present reaction model. On the other hand, for σ_{-1p} one finds a significant difference between the two sets of results. As mentioned above, the E_{in} dependence of σ_{-1p} at high energies is expected to be governed by that of σ_{pp} . The experimental data show a completely different E_{in} dependence. It will be very interesting and important to understand the origin of this behavior of the experimental data.

D. Neutron-induced one-nucleon knockout cross sections

Figures 6 and 7 show the results for $^{93}\text{Zr}(n, n'x)$, in the same way as in Figs. 3 and 4, respectively. In comparison with the results for $^{93}\text{Zr}(p, p'x)$ one sees that the E_{in} depen-

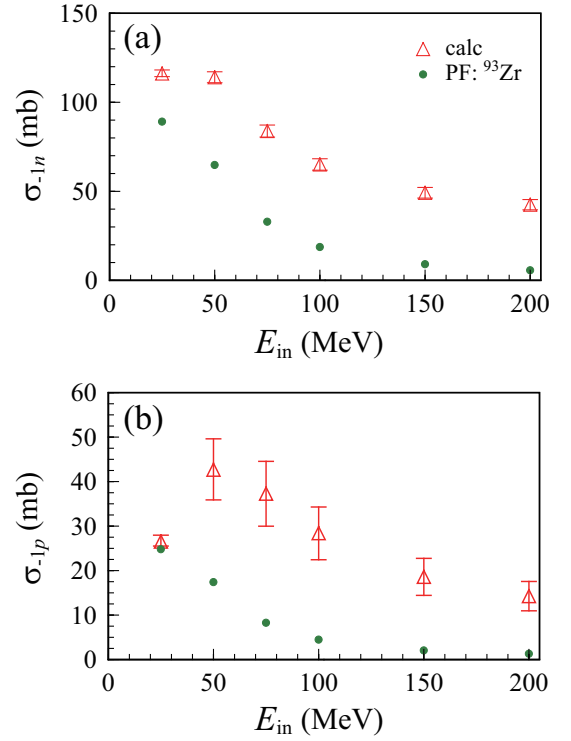


FIG. 6: (Color online) Same as in Fig. 3 but for $^{93}\text{Zr}(n, n'x)$.

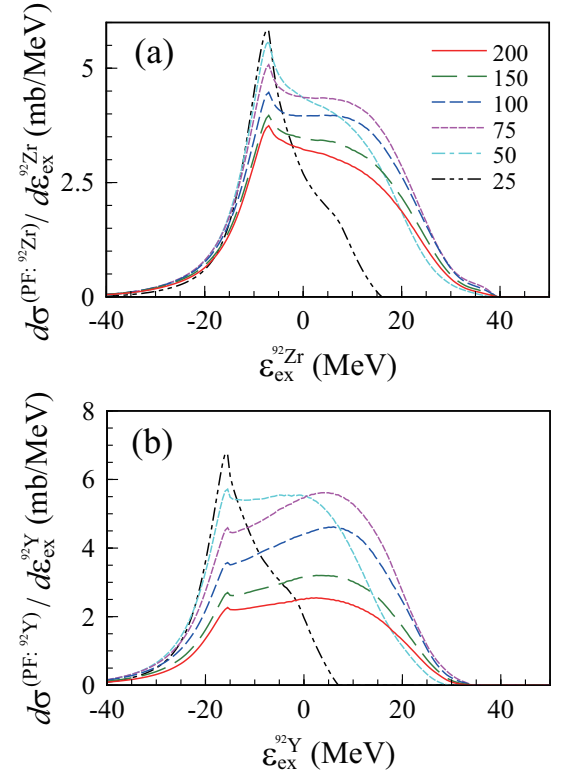


FIG. 7: (Color online) Same as in Fig. 4 but for $^{93}\text{Zr}(n, n'x)$.

dence at low energies becomes weaker. This is mainly due to the absence of the Coulomb barrier for the LP. In fact, the peak height in each panel of Fig. 7 increases as E_{in} decreases, which indicates the energy dependence of σ_{nN_t} is stronger than that of the absorption caused by the neutron optical potential down to 25 MeV. Another finding is the difference in the E_{in} dependence at higher energy. σ_{-1p} depends on E_{in} more strongly than σ_{-1n} , which is opposite to the behavior for $(p, p'x)$. This can easily be understood by the difference in the roles of σ_{nn} and σ_{pn} ; for $(n, n'x)$ the former (latter) that has a weaker (stronger) E_{in} dependence contributes to σ_{-1n} (σ_{-1p}). This explains also the difference in the ratios $\sigma_{-1n}/\sigma_{-1p}$ for $(p, p'x)$ and $(n, n'x)$ except at low energies.

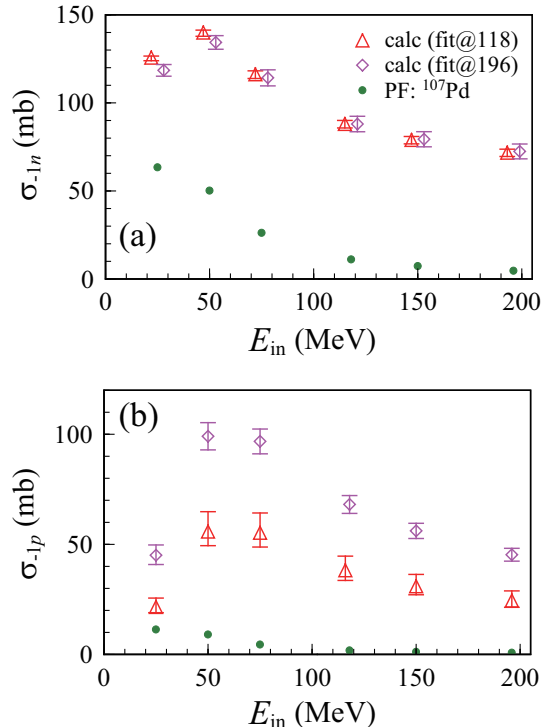


FIG. 8: (Color online) Same as in Fig. 5 but for $^{107}\text{Pd}(n, n'x)$.

Figure 8 shows the results for $^{107}\text{Pd}(n, n'x)$. Features of the results in comparison with those in Figs. 5 can be explained as in the same way as above. The calculated σ_{-1p} have large uncertainty, reflecting the difference between the two sets of $(\varepsilon_{0n}, \varepsilon_{0p})$.

IV. SUMMARY

I have proposed a reaction model for describing nucleon-induced inclusive one-nucleon knockout reactions. As an ad-

vantage to the existing INCL models, the model incorporates the WT of OBDM of a nucleus as a radial and momentum distribution of the struck nucleon inside the nucleus. The proposed model contains threshold parameters for the excitation energy distributions, ε_{0n} and ε_{0p} , which are determined so that the one-neutron (σ_{-1n}) and one-proton (σ_{-1p}) knockout cross sections reproduce the experimental data. These parameters are considered to reflect inadequacy of understanding of the nuclear many-body wave functions, those in the continuum states in particular.

After fixing the threshold parameters, the model has been applied to the study of the dependence of σ_{-1n} and σ_{-1p} on the incident energy E_{in} . At energies higher than about 75 MeV, the energy dependence is governed by that of the nucleon-nucleon total cross sections. This picture is supported by the experimental data for σ_{-1n} of $^{107}\text{Pd}(p, p'x)$ measured at 118 and 196 MeV, but contradicts the behavior of σ_{-1p} of the reaction. At low energies, because of the limitation of the energy transfer, it becomes difficult to knockout a target nucleon in general. However, the E_{in} dependence is determined by also that of the nuclear absorption and the Coulomb penetrability for the LP, and that of the nucleon-nucleon total cross sections. The E_{in} dependence of σ_{-1n} and σ_{-1p} for $(n, n'x)$ turned out to be quite different from that for $(p, p'x)$. This can be crucial for “extrapolating” proton-induced spallation cross sections to neutron-induced data that are inevitable for nuclear transmutation studies.

In this study I used a phenomenological s.p. wave functions of nuclei. Incorporation of more sophisticated nuclear wave functions calculated by, e.g., density functional theory will be desired. Combining a statistical model to describe decay of reaction residues is another important future work.

Acknowledgments

The author thanks M. Aikawa, S. Ebata, N. Furutachi, O. Iwamoto, S. Kawase, F. Minato, K. Minomo, T. Nakatsukasa, K. Niita, H. Otsu, H. Sakurai, S. Simoura, H. Wang, K. Washiyama, and Y. Watanabe for valuable discussions and comments. The computation was carried out with the computer facilities at the Research Center for Nuclear Physics, Osaka University. This work was supported in part by Grant-in-Aid of the Japan Society for the Promotion of Science (Grant No. JP16K05352) and by the ImPACT Program of the Council for Science, Technology and Innovation (Cabinet Office, Government of Japan).

[1] IAEA Technical Reports Series No. 435 (2004).

[2] H. Wang *et al.*, Phys. Lett. B **754**, 104 (2016).

- [3] H. Wang *et al.*, Prog. Theor. Exp. Phys. **2017**, 021D01 (2017).
- [4] S. Kawase *et al.*, Prog. Theor. Exp. Phys. **2017**, 093D03 (2017).
- [5] T. Sato, K. Niita, N. Matsuda, S. Hashimoto, Y. Iwamoto, S. Noda, T. Ogawa, H. Iwase, H. Nakashima, T. Fukahori, K. Okumura, T. Kai, S. Chiba, T. Furuta, L. Sihver, Particle and Heavy Ion Transport Code System PHITS, version 2.52, J. Nucl. Sci. Technol. 2013 Sep; 50: 913-923.
- [6] D. Mancusi, A. Boudard, J. Carbonell, J. Cugnon, J.-C. David, and S. Leray, Phys. Rev. C **91**, 034602 (2015).
- [7] A. Boudard, J. Cugnon, S. Leray, and C. Volant, Phys. Rev. C **66**, 044615 (2002).
- [8] A. Boudard, J. Cugnon, J.-C. David, S. Leray, and D. Mancusi, Phys. Rev. C **87**, 014606 (2013).
- [9] C. Paradela *et al.*, Phys. Rev. C **95**, 044606 (2017).
- [10] Y. L. Luo and M. Kawai, Phys. Rev. C **43**, 2367 (1991).
- [11] M. Kawai and H. A. Weidenmüller, Phys. Rev. C **45**, 1856 (1992).
- [12] Y. Watanabe, R. Kuwata, Sun Weili, M. Higashi, H. Shinohara, M. Kohno, K. Ogata, and M. Kawai, Phys. Rev. C **59**, 2136 (1999).
- [13] K. Ogata, M. Kawai, Y. Watanabe, Sun Weili, and M. Kohno, Phys. Rev. C **60**, 054605 (1999).
- [14] Sun Weili, Y. Watanabe, M. Kohno, K. Ogata, and M. Kawai, Phys. Rev. C **60**, 064605 (1999).
- [15] K. Ogata, Y. Watanabe, Sun Weili, M. Kohno, and M. Kawai, Nucl. Phys. A **703**, 152 (2002).
- [16] K. Ogata, Y. Watanabe, Sun Weili, M. Kohno, and M. Kawai, Proceedings of the Kyudai-RCNP International Symposium on Nuclear Many-Body and Medium Effects in Nuclear Interactions and Reactions, Fukuoka, 2002, World Scientific, Singapore, 2003, p. 231.
- [17] N. S. Chant and P. G. Roos, Phys. Rev. C **15**, 57 (1977).
- [18] N. S. Chant and P. G. Roos, Phys. Rev. C **27**, 1060 (1983).
- [19] T. Wakasa, K. Ogata, and T. Noro, Prog. Part. Nucl. Phys. **96**, 32 (2017).
- [20] R. Serber, Phys. Rev. **72**, 1114 (1947).
- [21] K. Niita, S. Chiba, T. Maruyama, T. Maruyama, H. Takada, T. Fukahori, Y. Nakahara, and A. Iwamoto, Phys. Rev. C **52**, 2620 (1995).
- [22] Y. Kanada-En'yo, M. Kimura, and A. Ono, Prog. Theor. Exp. Phys. **2012**, 01A202 (2012).
- [23] O. Iwamoto, N. Iwamoto, S. Kunieda, F. Minato, and K. Shibata, Nuclear Data Sheets **131**, 259 (2016).
- [24] S. Hama, B. C. Clark, E. D. Cooper, H. S. Sherif, and R. L. Mercer, Phys. Rev. C **41** 2737 (1990) ; E. D. Cooper, S. Hama, B. C. Clark, and R. L. Mercer, *ibid.* **47**, 297 (1993).
- [25] A. Bohr and B. R. Mottelson, *Nuclear Structure* (Benjamin, New York, 1969), Vol. I.
- [26] G. Perey and B. Buck, Nucl. Phys. **32**, 353 (1962).
- [27] C. Mahaux and R. Sartor, in *Advances in Nuclear Physics*, edited by J. W. Negele and E. Vogt (Plenum, New York, 1991) Vol. 20, p. 1.
- [28] M. A. Franey and W. G. Love, Phys. Rev. C **31**, 488 (1985).
- [29] M. Yahiro, K. Ogata, and K. Minomo, Prog. Theor. Phys. **126**, 167 (2011).